EARTHQUAKE SIMULATIONS ON A SELF-CENTERING STEEL MOMENT RESISTING FRAME WITH WEB FRICTION DEVICES

Ying-Cheng Lin[1], James Ricles[2], and Richard Sause[3]

[1] *Graduate Research Assistant, ATLSS Center, Department of Civil and Environmental Engineering, Lehigh University, 117 ATLSS Drive, Bethlehem, PA 18015, USA*

[2] *Bruce G. Johnston Professor of Structural Engineering, ATLSS Center, Department of Civil and Environmental Engineering, Lehigh University, Bethlehem, PA 18015, USA*

[3] *Joseph T. Stuart Professor of Structural Engineering, ATLSS Center, Department of Civil and Environmental Engineering, Lehigh University, Bethlehem, PA 18015, USA*

Email: ycl206@lehigh.edu, jmr5@lehigh.edu, rsause@lehigh.edu

ABSTRACT :

A self-centering moment resisting frame (SC-MRF) is a viable alternative to a conventional MRF for seismic resistant buildings. An SC-MRF is characterized by gap opening and closing at the beam-column interface under earthquake loading. The beams are post-tensioned to columns by high strength post-tensioning (PT) strands oriented horizontally to provide self-centering forces when gap opening occurs. For the SC-MRF investigated in this research, energy dissipation is provided by web friction devices (WFDs) on the beam. The PT strands and WFD each contribute to the moment capacity of the MRF connections. The SC-MRFs in this study are designed to meet several seismic performance objectives. These include no damage under the Design Basis Earthquake (DBE), leading to immediate occupancy performance following the DBE. In addition, under the Maximum Considered Earthquake (MCE) the structure is designed to have minimal damage and achieve the collapse prevention performance. A 7-bay, 4-story SC-MRF prototype building located on stiff soil in the Los Angeles area was designed with WFDs using a performance-based design procedure with the above performance objectives. A 0.6-scale model of two bays of the SC-MRFs was developed and tested at the NEES equipment site located at Lehigh University using the hybrid simulation method to include other parts of the building in the test. This paper presents an overview of the performance-based design procedure, the test results, and an assessment of the design procedure by a comparison of the test results with the expected performance of the SC-MRF.

KEYWORDS: Steel structures, self-centering MRF, post tensioning, web friction devices, beam-to-column connection, gap opening, hybrid simulation, performance-based design

1. INTRODUCTION

Conventional moment resisting frames (MRFs) are designed to dissipate energy under the design earthquake by developing damage in the members. This damage can result in large residual drift after the earthquake. To avoid large residual drift, post-tensioned (PT) beam-to-column connections for self-centering (SC) MRF were developed by Ricles et al. (2001). These connections develop a gap opening at the beam-column interface. The PT force enables the connection to self-center upon unloading. Energy dissipation occurs in special devices designed for the connection.

This paper presents an experimental study on a self-centering MRF (SC-MRF) with web friction devices (WFDs). The WFDs are used as energy dissipating devices and are positioned on the beam web to avoid interference with the floor slab. Using a performance based design (PBD) approach the SC-MRF is designed to be damage-free under the Design Based Earthquake (DBE) and enable immediate occupancy,

while also achieving the performance level of collapse prevention under the Maximum Considered Earthquake (MCE). Test results are presented and discussed to assess the design approach.

2. CONNECTION OVERVIEW AND BEHAVIOR

2.1. Connection Details

Figure 1(a) shows a SC-MRF with post-tensioned WFD (PT-WFD) beam-to-column connections. The PT strands are shown running parallel to the beams across multiple bays. A WFD connection, shown in Figure 1(b), includes two channel sections (referred to as friction channels) welded to column flange. Brass cartridge plates are sandwiched between the webs of the channels and beam to enable reliable friction to occur at their interface. The channels are clamped to the beam web by tightening the friction bolts shown in Figure 1(b) to produce the normal force on the friction surface. The channels are welded to the column flange after the friction bolts are tightened. The channel shape is selected to reduce the effect of weld shrinkage on the normal force on the friction surface. The shim plates shown in Figure 1(b) are welded to the column face to provide good contact surfaces for the beam flanges. Slotted holes are used in the beam web to accommodate the travel of the friction bolts during gap opening and closing of the connection. Reinforcing plates welded on the outside faces of the beam flanges are used to avoid excessive yielding in the beam flanges. Reinforcing plates are also welded to the inside faces of the column flanges to prevent low-cycle fatigue of the column flanges where holes for the PT strands are located. The reinforced net section area of each column flange is at least 85% of the flange gross area.

2.2. Moment-Rotation Behavior

The conceptual moment-relative rotation ($M\text{-}\theta_r$) behavior for a PT-WFD connection under cyclic loading is shown in Figure 1(c). From event 0 to 1, the connection has an initial stiffness that is similar to a conventional welded moment connection. Once the connection overcomes the imminent gap opening moment at event 1 ($M_{IGO,}$), where the M_{IGO} is the sum of the decompression moment M_d due to the initial PT force and the moment M_{Ff} due to friction in the WFD, the beam tension flange loses contact with the shim plate at the column face and gap opening occurs. After the M_{IGO} is overcome, the moment at the connection continues to increase as the PT force increases with strand elongation due to the gap opening (event 1 to 2). A large gap opening will eventually yield the PT strands at event 3. During unloading between events 2 and 4, θ_r remains constant but the connection moment decreases by $2M_{Ff}$ due to the reversal in direction of the friction force in the WFD. Continued unloading between events 4 and 5 reduces θ_r to zero as the beam tension flange comes in contact with the shim plate at the column face. Further unloading (between events 5 and 6) decreases the moment to zero as the beam tension flange fully compresses against the shim plate. A similar behavior occurs when a reversal in the applied moment occurs.

After gap opening, the moment M in the PT-WFD connection is controlled by the axial force P in the beam and friction force resultant F_f in the WFD, as follows:

$$M = Pd_2 + F_f r \tag{1}$$

In Eqn. (1) d_2 is the distance from the centroid of the beam section to the center of rotation (COR) of the connection, and r is the distance from the friction force resultant to the COR. The COR occurs at the point of contact of the compression beam flange with the column. Considering that a floor diaphragm force F_{fd} develops from the interaction of the SC-MRF with the floor system and the PT force T, the axial force in the beam P is (Garlock et al., 2005):

$$P = F_{fd} + T \tag{2}$$

where

$$T = T_o + \theta_r [2\, d_2\, k_b\, k_s / (k_b + k_s)] \quad (3)$$

In Eqn. (3) T_o is the initial PT force; and k_b and k_s are the axial stiffness of the beam and the PT strands within one bay, respectively.

3. PERFORMERCE BASED DESIGN

A performance-based design (PBD) procedure is used for the SC-MRF studied in this research. The PBD considers two levels of seismic hazard, namely the DBE and MCE. Under the DBE (which is equal to two-thirds the intensity of the MCE, and has an approximate 10% probability of being exceeded in 50 years) the SC-MRF is designed to achieve the immediate occupancy (IO) performance level defined in FEMA 450 (FEMA 2000), where limited structural and nonstructural damage occurs. Under the MCE (which has a 2% probability of being exceeded in 50 years), the collapse prevention (CP) performance level (FEMA 2000) should be achieved.

The design objectives and the limit states of the SC-MRF with PT-WFDs connections are shown in the conceptual base shear-roof drift ($V\text{-}\theta_{roof}$) response in Figure 2. Before the IO performance level, connection decompression and minimal yielding at the column bases of the SC-MRF is permitted to occur. Panel zone yielding, beam web yielding, and a beam flange strain greater than twice the yield strain is designed to occur between the IO and CP levels. At the CP level, PT strand yielding, beam web buckling, and excessive story drift are not permitted. The details of the design procedure are given in Garlock et al., (2005).

4. CONNECTION DESIGN

The effective energy dissipating ratio (β_E) of a PT-WFD connection expresses its energy dissipation characteristics. It can be shown that for a PT-WFD connection, the β_E can be determined as follows:

$$\beta_E = M_{Ff} / M_{IGO} \quad (4)$$

To enable a satisfactory response for the SC-MRF under seismic loading to be achieved, Seo and Sause (2005) recommend that $0.25 \leq \beta_E$. In addition, the target value of $M_{IGO} / M_{des} = 0.95$ is used, based on studies by Garlock (2002) and Rojas (2003). M_{des} is the design moment determined by an equivalent lateral force (ELF) analysis of the SC-MRF using a model of the MRF with rigid connections subject to the design forces associated with the design base shear V_{des} defined in ASCE7-05 by using the response modification factor R equal to 8.

5. EXPERIMENTAL PROGRAM

Using the design criteria and PBD approach described above, a 7x7-bay 4-story prototype building shown in Figure 3(a) was designed. The building is located on stiff soil in the Los Angeles. The perimeter frames include SC-MRFs. Each perimeter frame has two 2-bay SC-MRFs with PT-WFD connections. Figure 3(a) also shows the floor diaphragm is attached to one bay of each SC-MRF in each perimeter frame to avoid restraining the PT-WFDs connections from developing gap opening.

5.1. Test Structure and Test Setup

The test structure for the experimental program consisted of a 0.6-scale 4-story 2-bay SC-MRF with

PT-WFD connections, and is shown in Figure 3(b). A992 steel sections were used throughout the test structure. The member sizes are scaled down from the prototype structure. The test structure has W10x88 columns, W18x55 and W18x50 floor beams, and W14x34 roof beams. The Table 1 summarizes the SC-MRF design demands for roof drift (θ_{roof}), story drift (θ_s), and connection relative rotation (θ_r) under the DBE and MCE levels. The first mode period for the test structure is 1.23 second. The initial PT forces T_o, included in Figure 3(b), are less than 45% of ultimate strength (T_u). During the test, the lateral force at each level is applied through a floor diaphragm consisting of a loading beam system attached to the middle of the beam in the north bay by an actuator shown in Figure 3(b). The hybrid simulation method was used for the tests involving frequently occurring earthquake (FOE), DBE, and MCE tests discussed below. The test frame was the experimental substructure for the simulation. The gravity load bearing system and gravity loads tributary to the test structure were an analytical substructure in the hybrid simulation. The hybrid simulation used 2% damping in the 1st and 3rd modes, and an analytical model for the tributary mass of the test structure. The explicit unconditionally stable CR integration algorithm developed by Chen and Ricles (2008) was used to solve the equations of motion.

5.2. Test Matrix

Table 2 shows the test matrix. For the static tests, tests to obtain the stiffness matrix of the test frame and pushover tests to verify the behavior of the PT-WFD connections under cyclic loading were performed. The stiffness matrix was obtained by using the flexibility method.

For the hybrid simulation tests, ground motion records for FOE, DBE, and MCE levels were selected to assess the PBD method by comparing experimental results with the expected design objectives described previously. DBE-1 is a low-level DBE ground motion where no damage, including the column base yielding is expected to occur for DBE-1. From time history analysis, the expected value of roof drift, story drift, and connection relative rotation are about half of the design demands shown in Table 1. Tests with more demanding earthquake records (DBE-2, DBE-3, Aftershock, and MCE) are yet to be performed.

6. EXPERIMENTAL RESULTS

This paper focuses on the test results from DBE-1. Figure 4 shows the floor displacement time history from this test. The residual story drifts of the test frame are given in Table 3, and were obtained by dividing the difference between adjacent floor displacements by the story height. The maximum residual story drift is less than 0.2% radian, which demonstrates the self-centering capability of the SC-MRF.

Test results for DBE-1 test are shown in Table 4, and include maximum story drift $\theta_{s\,max}$, maximum relative rotation $\theta_{s\,max}$, maximum PT force T_{max} and residual PT force after the simulation $T_{o,DBE}$ normalized by the strand tensile strength T_u. The maximum $\theta_{s,max}$ is 1.9% radians and $\theta_{r,max}$ is 1.7% radians, which are about one-half of the expected design demand from Table 1 for the DBE. A plot of the PT force versus the average θ_r for each floor is given in Figure 5. The results show an increase in PT force when the gap opening occurs at the PT-WFD connections. The maximum PT forces for the DBE-1 test were $0.52T_u$ in the test (see Table 4). No yielding occurred in PT strands. The PT strand force decreased by a small amount during the test due to seating of the PT strand anchorage. Values for $T_{o,DBE}$ in Table 4 are less than the initial pre-stress level of $0.45T_u$.

The M-θ_r response for the 2nd floor south-bay beam connections are shown in Figure 6. The self-centering capability is demonstrated in Figure 6 where θ_r returns to zero upon unloading of the connection. After gap opening, the stiffness is different in the positive and negative moment directions. This is due to the effect of the floor diaphragm forces (i.e., the lateral force for the actuators) applied to the north bay beam. When structure is loaded to north direction, the floor diaphragm force imparts tension force in the south bay beam.

When structure is loaded to the south, the floor diaphragm imparts compression force in the south bay beam. Therefore, in Eq. (1) the axial force P in the south bay is different for the different loading directions. The estimated β_E is shown in Table 5 for each floor level, and was calculated by Eq. (4) using estimated M_{Ff} and M_{IGO} from the M-θ_r responses. Most of the floors have a β_E which is less than 25%, except for the 3rd floor. The low β_E indicated the friction forces in the WFDs were lower than the design target values, which were 24.3% for 1st floor, 25.5% for 2nd floor, 33.9% for 3rd floor, and 31.7% for the roof. In general, the WFD connections in the SC-MRF performed very well. Friction forces in the WFDs can be adjusted by retightening the friction bolts to provide greater energy dissipation.

7. SUMMARY AND CONCLUSIONS

The SC-MRF with PT-WFD connections performed well under the DBE-1 ground motion and in accordance with the objectives of the PBD. No damage occurred during the DBE-1. The test results demonstrate the self-centering capability of the SC-MRF. The WFDs are shown to provide energy dissipation, which can be adjusted by the amount of pretension in the friction bolts. Additional tests will be performed involving earthquake records that impose greater demand on the test structure. The PBD for the SC-MRF will be further assessed based on the results from these tests.

8. ACKNOWLEDGEMENTS

The research reported in this paper was conducted at the NEES Real-Time Multi-Directional (RTMD) Earthquake Testing Facility located at the ATLSS Center at Lehigh University. The work was supported by the National Science Foundation under Grant No. CMS-0420974, within the George E. Brown, Jr. Network for Earthquake Engineering Simulation Research (NEESR) program and Award No. CMS-0402490 NEES Consortium Operation.

REFERENCES

Chen, C., Ricles J.M. (2008), "Development of Direct Integration Algorithms for Structural Dynamics Using Discrete Control Theory," *Journal of Engineering Mechanics*, ASCE; 134:8, 676-683.

FEMA. (2000), *NEHRP Recommended Provisions for Seismic Regulations for New Buildings and Other Structures. Part 1 – Provisions and Part 2 – Commentary,* FEMA 450, Federal Emergency Management Agency, Washington, D.C.

Garlock, M. (2002), "Full-Scale Testing, Seismic Analysis, and Design of Post-Tensioned Seismic Resistant Connections for Steel Frames ," Ph.D. Dissertation, Civil and Environmental Engineering Dept., Lehigh University, Bethlehem, PA

Garlock M., Sause R., Ricles J.M. (2005), "Behavior and Design of Post-tensioned Steel Frame Systems," *Journal of Structural Engineering*, ASCE; 133:3, 389-399.

Ricles J.M., Sause R., Garlock M., Zhao C. (2001), "Post-Tensioned Seismic-Resistant Connections for Steel Frames," *Journal of Structural Engineering*, ASCE; 127:2, 113-121.

Rojas P. (2003), "Seismic Analysis, Design, and Evaluation of Post-tensioned Friction Damped Connections for Steel Moment Resisting Frames," Ph.D. Dissertation, Department of Civil and

Environmental Engineering. Lehigh University.

Seo, C-Y., Sause R. (2005), "Ductility Demands on Self-Centering Systems under Earthquake Loading," ACI Structural Journal; 102:2, 275-285.

Wolski M., Ricles J.M., Sause R. (2008), "Experimental Study of Self-centering Beam-column Moment Connections with a Bottom Flange Friction Device," *Journal of Structural Engineering*, submitted for publication.

Table 1 Design demands (in radians)

$\theta_{roof.,DBE}$	$\theta_{s.,DBE}$	$\theta_{r.,DBE}$	$\theta_{roof.,MCE}$	$\theta_{s.,MCE}$	$\theta_{r.,MCE}$
0.026	0.039	0.031	0.039	0.059	0.047

Table 2 Test matrix

Tests	Description	Ground Motion Record	Scale Factor	Test Method
Stiffness	Stiffness matrix determination	--	--	Static
Pushover	WFD connection behavior check	--	--	Static
FOE-1	1979 Imperial Valley	H-CXO225	0.700	Pseudo-dynamic
FOE-2	1979 Imperial Valley	H-CXO225	1.410	
DBE-1	1979 Imperial Valley	H-ECC002	0.943	
DBE-2	1989 Loma Prieta	SJTE315	1.533	
DBE-3	1994 Northridge	LOS000	1.182	
MCE	tbd	tbd	tbd	
Aftershock	tbd	tbd	tbd	

Table 3 Residual story drift after DBE-1 (in radian.)

Story	1st	2nd	3rd	4th
Drift	0.028%	0.082%	0.142%	0.187%

Table 4 Test results for DBE-1

Level	$\theta_{s\ max}$ (radians)	$\theta_{r\ max}$ (radians)	T_{max}/T_u (%)	$T_{o,DBE}/T_u$ (%)
RF	0.019	0.017	49	43
3F	0.018	0.015	47	38
2F	0.019	0.014	52	43
1F	0.012	0.014	51	44

Table 5 Estimated β_E for DBE-1

Level	1F	2F	3F	RF
β_E	22%	18%	28%	15%

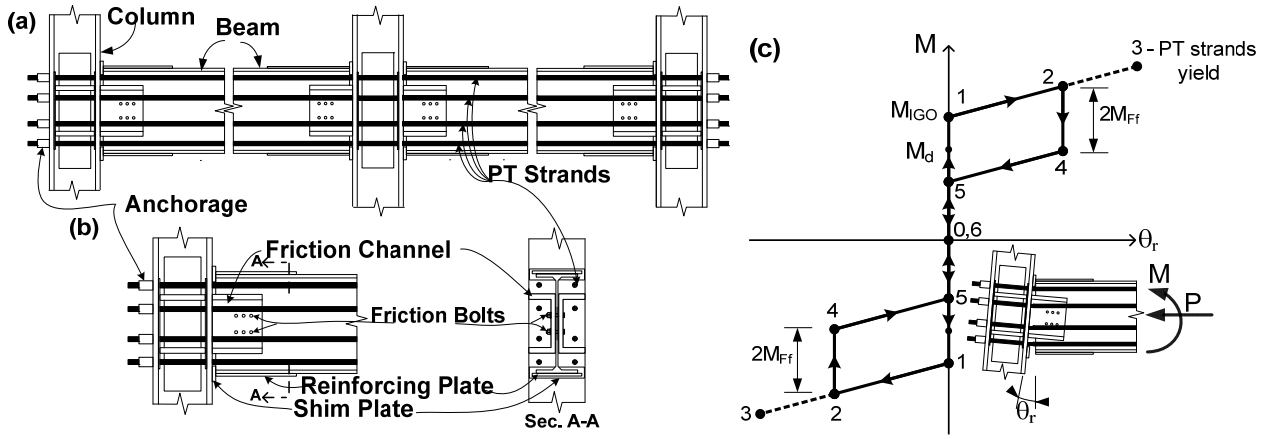

Figure 1 Schematic of (a) Elevation of a 2-bay SC-MRF with PT strands and WFDs, (b) Connection details, and (c) Conceptual moment-relative rotation (M-θ_r) behavior of connections with WFDs.

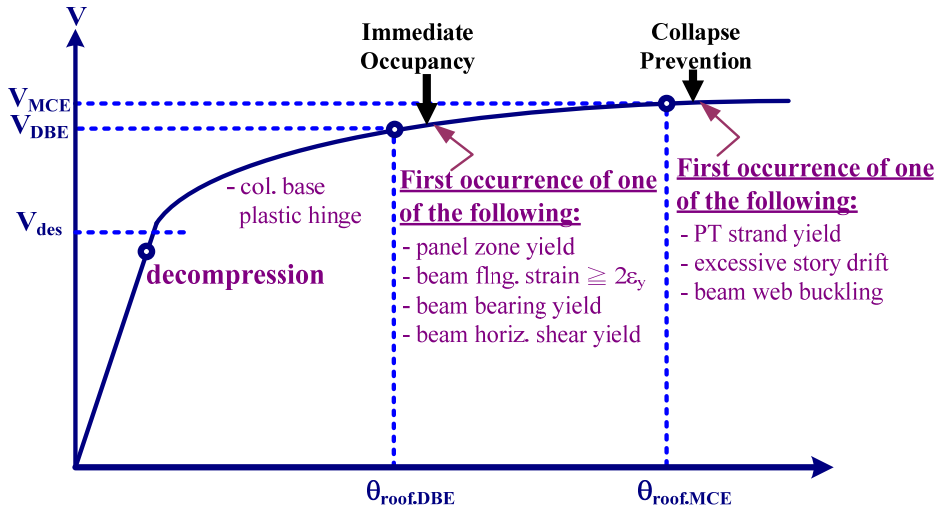

Figure 2 Performance based design objectives

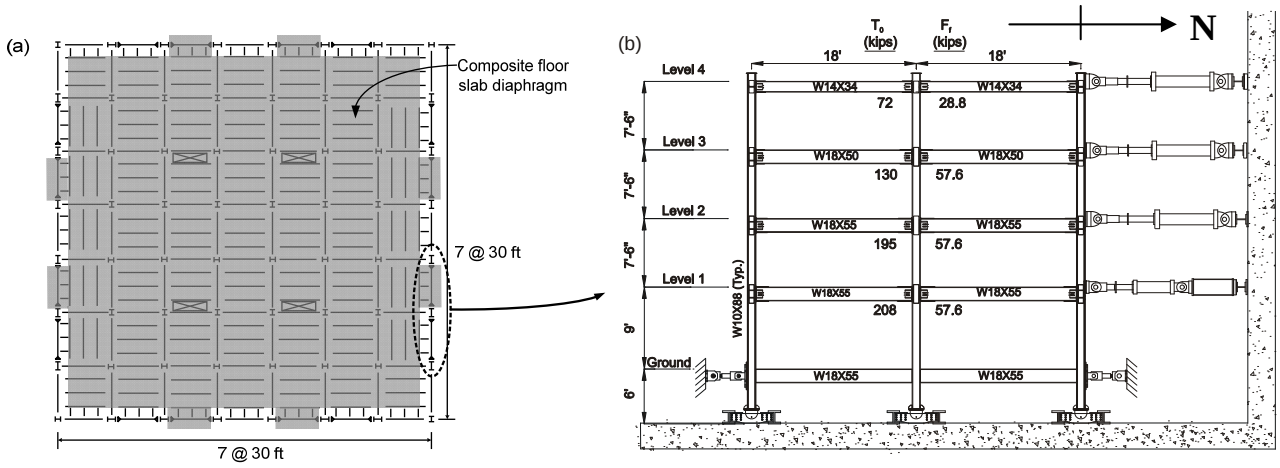

Figure 3 Schematic of (a) Plan of prototype, and (b) Elevation of 0.6-scale 4-story 2-bay SC-MRF test frame.

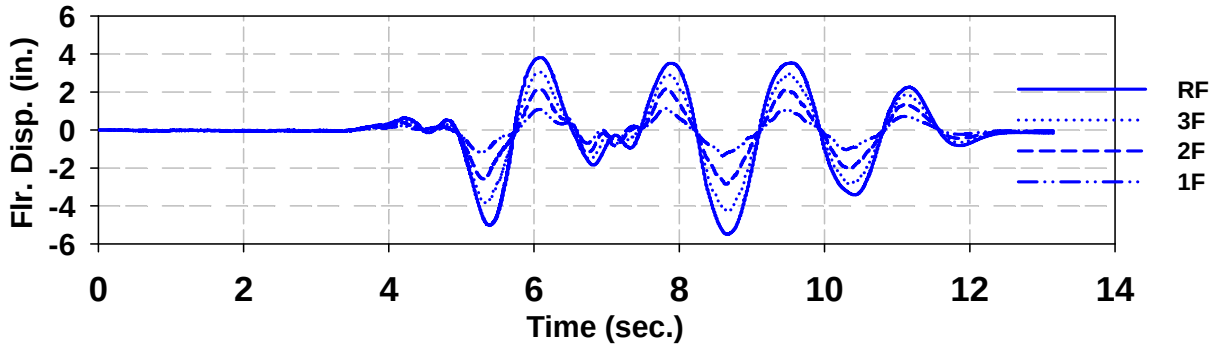

Figure 4 Floor displacements time history, DBE-1

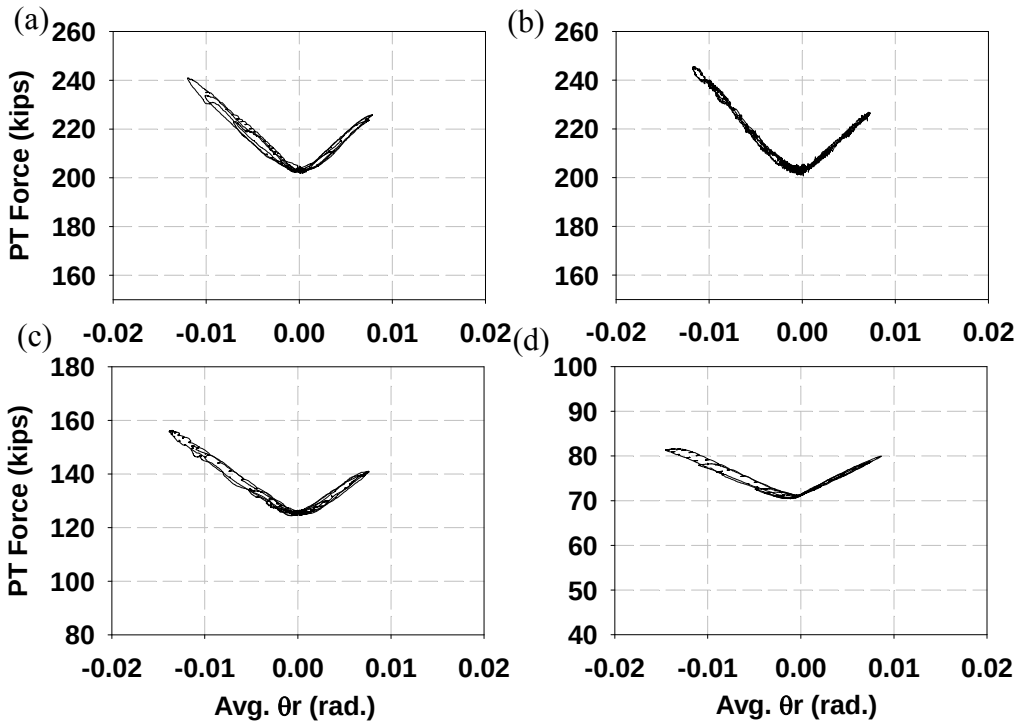

Figure 5 PT force vs. average θ_r, DBE-1 (a) 1st Floor; (b) 2nd Floor; (c) 3rd Floor; (d) Roof

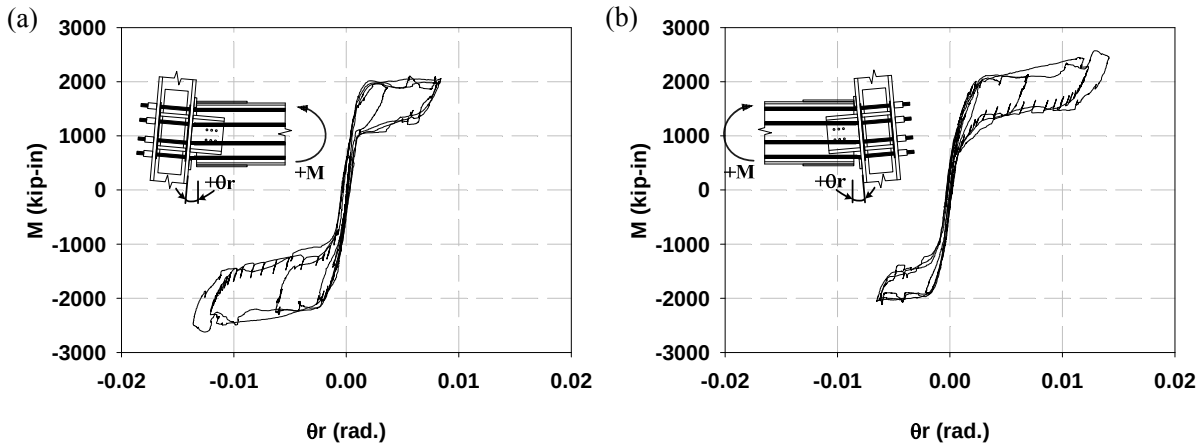

Figure 6 Moment vs. θ_r of (a) South-end connection and (b) North-end connection of the 2nd floor south-side beam, DBE-1